

Symmetric and asymmetric excitations of a strong-leg quantum spin ladder

D. Schmidiger, S. Mühlbauer, and A. Zheludev*

Neutron Scattering and Magnetism, Laboratory for Solid State Physics, ETH Zürich, Switzerland

P. Bouillot

Department of Medical Imaging and Information Sciences, Interventional Neuroradiology Unit, University Hospitals of Geneva, Geneva 1211, Switzerland and Laboratory for Hydraulic Machines, Ecole Polytechnique Fédérale de Lausanne, 1015 Lausanne, Switzerland

T. Giamarchi

DPMC-MaNEP, University of Geneva, Geneva, Switzerland

C. Kollath

HISKP, Universität Bonn, Nussallee 14-16, D-53115 Bonn, Germany

G. Ehlers

Quantum Condensed Matter Division, Oak Ridge National Laboratory, Oak Ridge, Tennessee 37831, USA

A. M. Tsvelik

Department of Condensed Matter Physics and Materials Science, Brookhaven National Laboratory, Upton, New York 11973-5000, USA

(Received 7 June 2013; revised manuscript received 15 August 2013; published 9 September 2013)

The zero-field excitation spectrum of the strong-leg spin ladder $(\text{C}_7\text{H}_{10}\text{N})_2\text{CuBr}_4$ is studied with a neutron time-of-flight technique. The spectrum is decomposed into its symmetric and asymmetric parts with respect to the rung momentum and compared with theoretical results obtained by the density matrix renormalization group method. Additionally, the calculated dynamical correlations are shown for a wide range of rung and leg coupling ratios in order to point out the evolution of arising excitations, as, e.g., of the two-magnon bound state from the strong to the weak coupling limit.

DOI: [10.1103/PhysRevB.88.094411](https://doi.org/10.1103/PhysRevB.88.094411)

PACS number(s): 75.10.Jm, 75.10.Kt, 75.40.Gb

I. INTRODUCTION

The discovery of materials as clean realizations of quasi-one-dimensional spin Hamiltonians enabled the study of one-dimensional many-body physics^{1,2} and fascinating phenomena such as Luttinger-liquid behavior³⁻⁶ or (quantum) phase transitions of gapped quantum magnets,⁷⁻¹⁰ in quantitative agreement with theoretical and numerical predictions. Among these systems, the Heisenberg antiferromagnetic (AF) two-leg spin ladder¹¹ belongs to the simplest models, yet features nontrivial physics. Recently the possibility to control such systems with the application of a magnetic field large enough to induce sizable changes in the magnetization has allowed us to explore a huge variety of physical phenomena.¹²

Lately, a lot of effort was put in the study of dimerized *strong-rung* spin ladders, such as, e.g., the organometallic compounds $(\text{CH}_3)_2\text{CHNH}_3\text{CuCl}_3(\text{IPA-CuCl}_3)$ ^{10,13,14} or $(\text{C}_5\text{H}_{12}\text{N})_2\text{CuBr}_4(\text{BPCB})$.^{6,7,15,16} In this coupling limit the zero-field excitation spectrum is dominated by gapped but hardly mobile dimer triplet excitations on the rung. Nowadays, the basic underlying physics at zero magnetic field can be regarded as well established: Analytical solutions are provided by, e.g., the strong-coupling approach,^{17,18} starting from noninteracting dimers.

In contrast, the physics of *strong-leg* spin ladders remained much more elusive, mainly due to the lack of suitable analytic approaches, in particular for the regime $J_{\text{rung}}/J_{\text{leg}} \approx 1$. The

existence of the spin liquid ground state and the widely dispersive gapped magnon is less obvious and originates in a subtle Haldane mechanism.^{19,20}

In contrast to the *strong-rung* limit, two-magnon excitations become progressively more important. The strong but short-ranged attractive potential between magnons leads to pronounced two-magnon bound states below a two-magnon continuum. So far, two-magnon excitations in spin ladders were observed in the cuprate material $\text{La}_4\text{Sr}_{10}\text{Cu}_{24}\text{O}_{41}$ ²¹ and more recently in the organometallic low-energy scale material $(\text{C}_7\text{H}_{10}\text{N})_2\text{CuBr}_4$ (DIMPY^{22,23}). In this work we study one- and two-magnon excitations in the latter material with a complementary technique and thereby extend the measurements of Refs. 24 and 25.

DIMPY is currently the cleanest²⁶ realization of a *strong-leg* spin-ladder material. It crystallizes in a monoclinic structure with space group $P2(1)/n$ and lattice constants²² $a = 7.504 \text{ \AA}$, $b = 31.61 \text{ \AA}$, $c = 8.202 \text{ \AA}$, and $\beta = 98.98^\circ$. Cu^{2+} ions with an effective spin $S = 1/2$ in a tetrahedral environment of Br^- ions are interacting through Cu-Br-Br-Cu superexchange pathways, thereby building a ladderlike spin network (Fig. 1). DIMPY features two different ladder systems, both running along the crystallographic \mathbf{a} axis but being described by distinct rung vectors $\mathbf{d}_{1,2} = (0.423, \pm 0.256, 0.293)$, in fractional coordinates.²² Recent zero-field triple-axis neutron scattering experiments in combination with DMRG calculations indicated that the

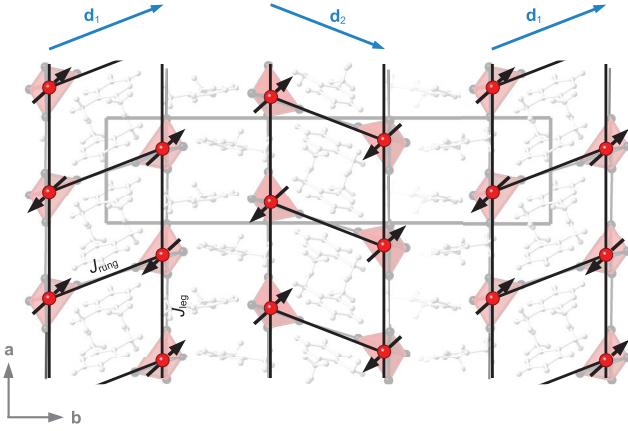


FIG. 1. (Color online) Illustration of the crystallographic structure of $(\text{C}_7\text{H}_{10}\text{N})_2\text{CuBr}_4$ (DIMPY), projected onto the (a, b) plane. Cu^{2+} and Br^- ions are shown as red and black spheres, respectively. The two ladder systems as well as the relevant interactions are shown, together with the corresponding rung vectors $\mathbf{d}_{1,2}$ (blue arrows).

low-energy physics is governed by the Heisenberg spin-ladder Hamiltonian

$$\mathcal{H} = J_{\text{leg}} \sum_l \sum_{j=1}^2 \mathbf{S}_{l,j} \cdot \mathbf{S}_{l+1,j} + J_{\text{rung}} \sum_l \mathbf{S}_{l,1} \cdot \mathbf{S}_{l,2}. \quad (1)$$

Neutron experiments in combination with PCUT calculations estimated $J_{\text{leg}}/J_{\text{rung}} \approx 2.2(2)$, while careful measurements of the magnon dispersion²⁴ in combination with density matrix renormalization group (DMRG) calculations²⁵ determined the exchange constants to be $J_{\text{leg}} = 1.42(6)$ meV and $J_{\text{rung}} = 0.82(2)$ meV. Additional intraladder interactions were found to be insignificant,²⁴ while low-temperature specific heat measurements²⁵ estimated interladder interactions to be on the order of $6 \mu\text{eV}$. In the following, the theoretical calculations are performed using the time-dependent DMRG method with J_{rung} and J_{leg} as quoted above. For details on the calculations we refer to Ref. 25.

Due to the absence of, e.g., diagonal interactions, the spin Hamiltonian possesses leg-permutation symmetry and the total dynamical structure factor $\mathcal{S}(\mathbf{q}, \omega)$ decomposes into a symmetric $\mathcal{S}_+(\mathbf{q}, \omega)$ and asymmetric $\mathcal{S}_-(\mathbf{q}, \omega)$ part,²⁴

$$\mathcal{S}(\mathbf{q}, \omega) = s^+(\mathbf{q}) \mathcal{S}_+(\mathbf{q}, \omega) + s^-(\mathbf{q}) \mathcal{S}_-(\mathbf{q}, \omega), \quad (2)$$

where $s^-(\mathbf{q})$ and $s^+(\mathbf{q})$ denote the asymmetric and symmetric structure factor, respectively. Assuming the two ladder systems with $\mathbf{d}_{1,2}$ to be noninteracting, they are given by

$$4s^\pm(\mathbf{q}) = 2 \pm \cos(\mathbf{q} \cdot \mathbf{d}_1) \pm \cos(\mathbf{q} \cdot \mathbf{d}_2). \quad (3)$$

Odd and even number of magnon excitations contribute to the asymmetric and symmetric channel, respectively.

In neutron scattering experiments, the partial differential cross section is measured. For magnetic scattering as discussed in this work, it is given by²⁷

$$\frac{d^2\sigma}{d\Omega d\omega} \propto N \frac{k_f}{k_i} |F(\mathbf{q})|^2 \mathcal{S}(\mathbf{q}, \omega), \quad (4)$$

where N denotes the number of unit cells in the sample, $F(\mathbf{q})$ is the magnetic form factor, \mathbf{k}_i (\mathbf{k}_f) is the wave vector of the incident (final) neutrons, and $\mathbf{q} = \mathbf{k}_f - \mathbf{k}_i$ is the momentum transfer. The latter can be written as $\mathbf{q} = h\mathbf{a}^* + k\mathbf{b}^* + l\mathbf{c}^*$, with \mathbf{a}^* , \mathbf{b}^* , and \mathbf{c}^* describing the reciprocal lattice vectors of the crystal. Due to the different structure factors of the symmetric and asymmetric channel, symmetric and asymmetric excitations can be fully separated in a neutron scattering experiment.

In recent experiments, the single magnon dispersion was measured by triple-axis neutron scattering and found to be persisting throughout the complete Brillouin zone, confirming the leg-permutation symmetry.²⁴ In subsequent triple-axis experiments, a two-magnon bound state was observed by performing scans at three positions in reciprocal space, $(h, k, l) = (\eta, 0, -1.44 \cdot \eta)$, with $\eta = 0.5, 0.625, \text{ and } 0.75$, quantitatively confirming numerical density matrix renormalization group (DMRG) calculation of $\mathcal{S}_+(\mathbf{q}, \omega)$.²⁵

The goal of this work is twofold: First, we extend the measurements of Refs. 24 and 25 by using the complementary neutron time-of-flight (TOF) technique, since a detailed analysis of the symmetric and asymmetric zero-field spectrum of DIMPY has not yet been performed. We study the bound state in detail, definitely prove the leg-permutation symmetry, and separate the symmetry channels completely. Second, DMRG calculations of the dynamical structure factor were performed for different coupling ratios $0.5 < J_{\text{leg}}/J_{\text{rung}} < \infty$. This enables us to numerically observe the evolution of excitations from the strong-rung to the strong-leg regime and to compare it to existing analytic results.

II. EXPERIMENT

For the present experiment, the same sample as in Refs. 24 and 25 was used. It consisted of four fully deuterated single crystals $(\text{C}_7\text{D}_{10}\text{N})_2\text{CuBr}_4$ with a total mass of 3.7 g and co-aligned to a mosaic spread better than 1.5° . Measurements were performed at the CNCS cold neutron chopper spectrometer²⁸ at SNS spallation source. Temperature was controlled with a conventional ^4He cryostat and the sample was mounted with the \mathbf{b} axis vertical. Measurements were performed at $T = 1.5$ K and background data was collected at 50 and 110 K. The incident energy was fixed to 4.2 meV and the sample was rotated by 180° in steps of 5° . Intensity was normalized to the proton charge on the target: $1.5 \mu\text{C}$ (40 min counting time) per rotation step for the 1.5 K and $0.75 \mu\text{C}$ for the 50 and 110 K measurements, respectively.

III. RESULTS AND DISCUSSION

A. Integrated intensity and structure factor

Due to the exceptional one-dimensional nature of DIMPY, no dispersion along the perpendicular directions \mathbf{b}^* and \mathbf{c}^* was observed previously.²⁹ Neutron time-of-flight data can hence be integrated along these directions, thereby improving statistics. Raw data at $T = 1.5$ and 50 K, integrated along \mathbf{b}^* and \mathbf{c}^* using the Horace program³⁰ is shown in Figs. 2(a) and 2(b).

At 1.5 K both the single-magnon excitation and the two-magnon bound state are observed over four Brillouin zones. However, the magnetic signal is contaminated by

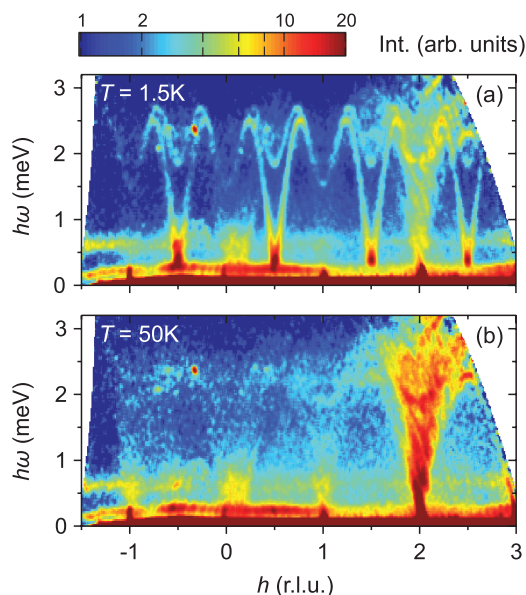


FIG. 2. (Color online) Raw data from neutron time-of-flight experiments in $(\text{C}_7\text{D}_{10}\text{N})_2\text{CuBr}_4$, measured at (a) $T = 1.5$ K and (b) $T = 50$ K. Data was integrated along the nondispersive \mathbf{b}^* and \mathbf{c}^* direction. Intensity is shown as a function of energy transfer $\hbar\omega$ and momentum transfer along the leg h , in reciprocal lattice units.

T -dependent and T -independent contributions. The T -dependent contributions are mainly due to the inelastic phonon scattering. This is in contrast to T -independent background, which can stem from both coherent and incoherent scattering by the sample and equipment. Such contributions are evident in comparison with the measurement at 50 K [Fig. 2(b)].

Background subtraction was performed taking both of these contributions into account as described in the Appendix, using the integrated data sets. In Fig. 3 background subtracted data is shown in the Brillouin zone $0 < h < 1$. Clearly most of the background features are removed by our procedure.

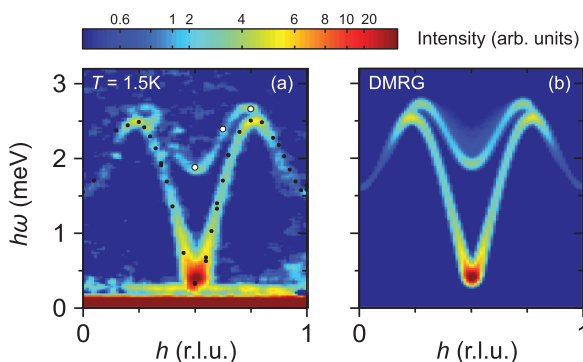


FIG. 3. (Color online) (a) Background subtracted data from neutron time-of-flight experiments in $(\text{C}_7\text{D}_{10}\text{N})_2\text{CuBr}_4$, integrated along the \mathbf{b}^* and \mathbf{c}^* direction. Intensity is shown as a function of energy transfer $\hbar\omega$ and momentum transfer along the leg. Black and white points correspond to triple-axis measurements of the magnon and two-magnon bound state excitations (Refs. 24 and 25). (b) Numerical DMRG calculation of the dynamical structure factor $\mathcal{S}_+(h, \omega) + \mathcal{S}_-(h, \omega)$, convoluted with experimental resolution. The measured and calculated spectra show remarkable agreement.

Due to the integration process, the cosine functions in Eq. (3) average to zero and an equal combination of $\mathcal{S}_+(h, \omega)$ and $\mathcal{S}_-(h, \omega)$ is observed. The measured magnon dispersion agrees with the recently performed triple-axis experiment at $T = 50$ mK (black points, from Ref. 24). Moreover, the two-magnon bound state clearly persists in the region $0.2 < h < 0.8$ and is consistent with the three constant- \mathbf{q} scans performed in Ref. 25 (white points), while two-magnon continuum excitations are too weak to be observed under experimental conditions. The numerical calculation of $\mathcal{S}_+(h, \omega) + \mathcal{S}_-(h, \omega)$ convoluted with an approximate experimental resolution [Fig. 3(b)] is in quantitative agreement with the experiment, both in terms of dispersion and intensity of the two sharp modes.

In order to map out the structure factors $s^\pm(\mathbf{q})$, raw data at 1.5, 50, and 110 K was integrated around the magnetic zone center $h = [0.45, 0.55]$ rlu and in the energy range $\hbar\omega = [0.2, 0.6]$ and $[1.75, 2.05]$ meV, enclosing the magnon and two-magnon bound states, respectively. As described in the Appendix, the instrumental and phonon background were separated, extrapolated to 1.5 K, and subtracted [Figs. 4(a) and 4(c)].

The structure factors $s_h^\pm(k, l)$ given by Eq. (3) were calculated for $h = 0.5$ on the same k, l grid as experimental data [Figs. 4(b) and 4(d)]. They were multiplied by the magnetic form factor of the Cu^{2+} ion, given by $|F_h(k, l)|^2 \approx |\langle j_0 \rangle_h(k, l)|^2$, and with the function j_0 as numerically calculated in Ref. 31.

The cut around the single magnon excitation [Fig. 4(a)] clearly follows the predicted asymmetric channel structure factor $s_h^-(k, l)$ [Fig. 4(b)]. Although the vertical coverage of a 2D time-of-flight detector is limited by $\pm 16^\circ$, the exceptionally

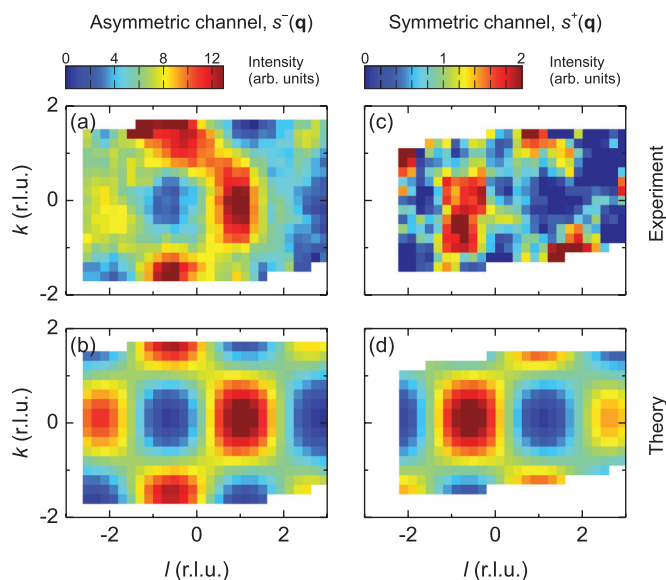


FIG. 4. (Color online) Background subtracted data $\mathcal{T}_h^{\text{sub}}(k, l)$ as a function of momentum transfer along the perpendicular directions \mathbf{b}^* and \mathbf{c}^* , in order to visualize (a) the asymmetric and (c) the symmetric structure factors $s_h^\pm(k, l)$. Data was integrated along $h = [0.45, 0.55]$ rlu and in the energy range (a) $\hbar\omega = [0.2, 0.6]$ meV and (c) $[1.75, 2.05]$ meV. The corresponding calculation of the asymmetric and symmetric structure factor $s_h^\pm(k, l)$ weighted by the magnetic form factor are shown in (b) and (d).

long \mathbf{b} axis of DIMPY ($b = 31.61 \text{ \AA}$) enables us to observe a full period of the structure factor in a vertical direction.

Although the signal for the cut around the two-magnon bound state [Fig. 4(c)] is much weaker, we observe enhanced intensity in the range $-2 < l < 0$, with $-1 < k < 1$, while it is basically zero for $0 < l < 2$. This is in agreement with the calculated variation of the symmetric structure factor $s_h^+(k, l)$ as shown in Fig. 4(d). The assumption of two noninteracting ladder systems with structure factors as in Eq. (3) is hence found to be valid.

B. Channel separation

As a next step, the two symmetry channels were separated. The basic idea was to divide the 4D data set of 2D cuts by integrating along small ranges in h and $\hbar\omega$ and to determine the contribution of the asymmetric and symmetric channel for each value of h_i and $\hbar\omega_i$, assuming that the structure factors are given by Eq. (3).

The h - $\hbar\omega$ plane was divided into 1600 boxes ($h_i, \hbar\omega_i$) of the size $0.025 \text{ rlu} \times 0.075 \text{ meV}$. For each box ($h_i, \hbar\omega_i$), data measured at 1.5, 50, and 110 K was integrated along a small range $h_i \pm 0.025 \text{ rlu}$ and $\hbar\omega_i \pm 0.075 \text{ meV}$, leaving 2D data sets $\mathcal{I}_{h_i, \omega_i}^T(k, l)$. Background subtraction was performed for each ($h_i, \hbar\omega_i$) using the data sets $\mathcal{I}_{h_i, \omega_i}^T(k, l)$, with $T = 1.5, 50$, and 110 K, as described in the Appendix.

The structure factor for the asymmetric and symmetric channel $s_{h_i}^\pm(k, l)$ were calculated on the same grid as the data. Two masks $M_{h_i, \omega_i}^\pm(k, l)$ were defined by

$$M_{h_i, \omega_i}^\pm(k, l) = \begin{cases} s_{h_i, \omega_i}^\pm(k, l)^{-1} |F_{h_i}(k, l)|^{-2}, & s_{h_i, \omega_i}^\pm(k, l) \geq L_\pm, \\ 0, & \text{else,} \end{cases} \quad (5)$$

such that the asymmetric and symmetric masks $M_{h_i, \omega_i}^\pm(k, l)$ cut out data in the region where intensity from the corresponding channel is expected by the structure factor. The threshold for the channel were taken to be $L_+ = 0.8$ and $L_- = 0.85$, respectively.³²

In order to determine the asymmetric contribution, background subtracted data $\mathcal{I}_{h_i, \omega_i}^{\text{sub}}(k, l)$ was multiplied elementwise by the asymmetric mask $M_{h_i, \omega_i}^-(k, l)$, summed up and divided by the number of nonzero elements—leaving one number $I^-(h_i, \omega_i)$ describing the asymmetric contribution at the position (h_i, ω_i). The same procedure was performed for the symmetric mask $M_{h_i, \omega_i}^+(k, l)$ leading to the symmetric contribution $I^+(h_i, \omega_i)$ at (h_i, ω_i).

The separated and symmetrized contributions $I^-(h, \omega)$ and $I^+(h, \omega)$ in the first Brillouin zone $0 < h < 1$ are shown in Figs. 5(a) and 5(c), respectively. $I^-(h, \omega)$ clearly contains the single-magnon excitation while no contribution from the two-magnon bound state is visible. Figure 5(b) shows the DMRG calculation of $\mathcal{S}_-(h, \omega)$, convoluted with a similar resolution as in Fig. 5(a). However, due to the separation process, the intensity cannot be compared anymore. The two-magnon bound state is clearly visible in the separated even channel $I^+(h, \omega)$, in agreement with the calculated $\mathcal{S}_+(h, \omega)$ [Fig. 5(d)]. $I^+(h, \omega)$ still contains a “ghost” of the single-magnon excitation (black arrow), an artifact of the separation process.

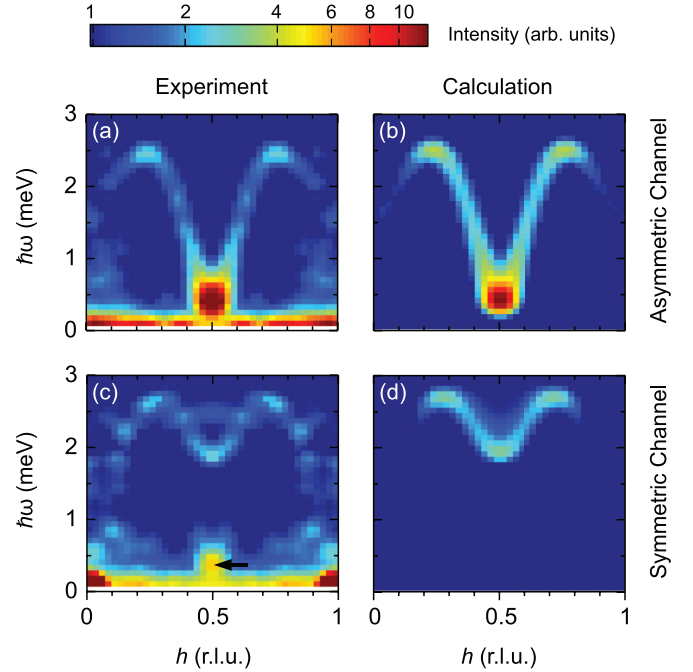


FIG. 5. (Color online) Separation of the asymmetric and symmetric channel in $(\text{C}_7\text{D}_{10}\text{N})_2\text{CuBr}_4$. (a) Asymmetric and (c) symmetric contribution extracted from raw data as explained in the text. A spurious remainder of the single-magnon excitation is still visible in the separated symmetric contribution (c) (black arrow). DMRG calculation of (b) $\mathcal{S}_-(h, \omega)$ and (d) $\mathcal{S}_+(h, \omega)$, convoluted with a similar resolution as in (a).

IV. DISCUSSION

The results can be summarized as follows. (1) The excitations spectrum of DIMPY is dominated by the well-known magnon excitation as well as a strong and highly dispersive two-magnon bound state, persisting throughout about 60% of the Brillouin zone. The intensity and dispersion of both modes are in full agreement with the DMRG calculations. (2) The symmetric and asymmetric structure factor follows the prediction for noninteracting ladder systems with rung vectors $\mathbf{d}_{1,2}$ and can directly be mapped out in a TOF experiment. (3) DIMPY features the leg-permutation symmetry. The asymmetric and symmetric excitation channel can be fully separated. The former contains the magnon excitation, while the latter contains the two-magnon bound state.

In order to put the results into context, we show in the following DMRG calculations of the momentum and frequency resolved dynamical structure factor in both symmetry channels from the strong-rung to the strong-leg regime. This enables us to relate to numerous aspects of the spin-ladder problem in either coupling regimes which were studied in detail before, both analytically and numerically.^{20,33–39}

The calculations were performed for different coupling ratios $x = J_{\text{leg}}/J_{\text{rung}}$, particularly for $x = 0.5, 1, 1.72, 5, 10$, with J_{leg} fixed to unity, as well as for the spin chain ($x \rightarrow \infty$). Figure 6 shows the calculated structure factor in the asymmetric (*left*) and symmetric (*right*) channel for different coupling ratios. It is shown as a function of energy $\hbar\omega$ and momentum along the leg of the ladder $q_{\parallel} := \mathbf{q} \cdot \mathbf{a}$.

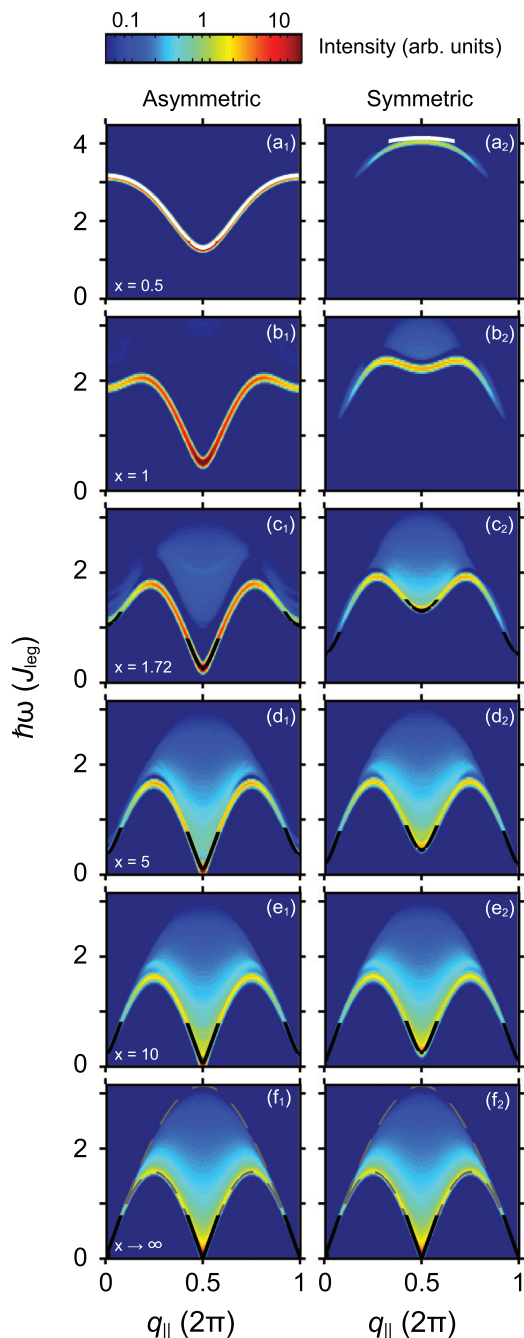


FIG. 6. (Color online) DMRG calculation of the dynamic structure factor in the asymmetric (left, $q_{\perp} = \pi$) and symmetric (right, $q_{\perp} = 0$), as a function of $x = J_{\text{leg}}/J_{\text{rung}}$. White lines correspond to predictions from Refs. 36 and 37. Black lines indicate the boundaries of multiparticle continua as described in the text.

In the strong-rung regime with $x < 1$ [Figs. 6(a) and 6(b)], the spin ladder consists of weakly interacting dimers. The asymmetric dynamical structure factor is dominated by an almost dispersionless magnon excitation with a gap $\Delta \simeq J_{\text{rung}} - J_{\text{leg}}$ and a bandwidth $W \simeq 2J_{\text{leg}}$. The symmetric channel contains a weak two-magnon continuum as well as a $S = 1$ bound state existing in a narrow region around the magnetic zone center $q_{\parallel} = \pi$.

For strong-rung ladders, the dispersion³⁷ and the spectral weight of the magnon, the two-magnon continuum, as well as the bound states were calculated using the strong-coupling expansion^{33,35,38} and with the linked cluster series expansion.³⁶ White lines in Fig. 6(a) correspond to the calculation in Refs. 36 and 37 and agree for $x = 0.5$. Moreover, the results indicate that for $x \rightarrow 0$, the triplet bound state exists only in a narrow q range with $2\pi/3 < q_{\parallel} < 4\pi/3$ (i.e., in 1/3 of the Brillouin zone) and that the spectral weight of the triplet state scales with x^2 (Ref. 33). In strong-rung ladders, two-magnon excitations are hence usually too weak to be observable by neutron scattering methods.

In contrast, for the strong-leg coupling regime $x > 1$ both the symmetric and asymmetric dynamical structure factors converge towards the two-spinon continuum excitation spectrum of the Heisenberg $S = 1/2$ spin chain for $x \rightarrow \infty$ [Fig. 6(f)]. The latter is gapless, features a bandwidth of $W = \pi J_{\text{leg}}$, and is bounded⁴⁰ by $\epsilon_1 = \pi J_{\text{leg}}/2 |\sin(q_{\parallel})|$ and $\epsilon_u = \pi J_{\text{leg}} |\sin(q_{\parallel}/2)|$ [gray broken lines in Fig. 6(f)].

At finite interchain interaction J_{rung} , spinons are confined and asymmetric excitations acquire a spin gap of $\Delta \simeq 0.41 J_{\text{rung}}$ if $x \gg 1$ (Ref. 34). As pointed out by Shelton *et al.*,⁴¹ the bosonized Hamiltonian can be mapped onto a system of weakly interacting massive triplet and singlet Majorana fermions, with masses $m_s \simeq 3m_t$ and with the velocity of the Heisenberg spin chain $v = \pi J_{\text{leg}}/2$. The triplet Majorana fermion is asymmetric under leg permutation symmetry (its rung momentum is $q_{\perp} = \pi$), while the singlet Majorana fermion is symmetric with $q_{\perp} = 0$. The dynamic structure factor contains various sharp and continuous single and multi-Majorana fermion excitations, summarized in Table I.

The triplet excitation (the ‘‘magnon’’) is a sharp mode around $q_{\parallel} = \pi$ only and its dispersion is described by

$$\epsilon_t = \sqrt{m^2 + v^2(q_{\parallel} - \pi)^2}, \quad (6)$$

with $m \approx 0.41 J_{\text{rung}}$. The lower boundaries of the multiparticle continua are given by

$$\epsilon_1 = \sqrt{m_{\text{thresh}}^2 + v^2(q_{\parallel} - q_{\parallel, \text{min}})^2} \quad (7)$$

and can be observed either in the symmetric ($q_{\perp} = 0$) or asymmetric ($q_{\perp} = \pi$) channel. These predictions are shown as black full lines in Figs. 6(c)–6(f) and successfully describe the lower boundary of the dynamical structure factor in the strong-leg regime, confirming the analytical predictions. In particular, in the symmetric channel, the continuum around

TABLE I. Multitriplet (T) and singlet (S) low energy excitations. The rung q_{\perp} denotes the symmetry channel in which these excitations appear, while $q_{\parallel, \text{min}}$ determines whether they occur around π or 0. m_{thresh} describes the gap of the corresponding excitation.

Excitation	q_{\perp}	$q_{\parallel, \text{min}}$	Threshold m_{thresh}
1T	π	π	$1m$
2T	0	0	$2m$
3T	π	π	$3m$
1T + 1S	π	0	$4m$
2T + 1S	0	π	$5m$

$q_{\parallel} = \pi$ corresponds to two triplet and one singlet excitation, whereas the continuum around $q_{\parallel} = 0$ results from two triplet excitations.

For the experimental value $x \approx 1.72$ in DIMPY instead of the threshold singularity the symmetric channel displays a rather well defined coherent mode. In the framework of Ref. 41 this corresponds to the three-particle bound state of two triplet and one singlet excitation. This value of x is too small for the above theory to yield good quantitative predictions, though it contains a provision for such a bound state. This provision comes in the form of the interaction of the Majorana fermions originating from the coupling of uniform magnetizations of the two chains.⁴¹ The massive Majorana fermions interact and with the proper sign of interaction can create bound states. Nevertheless, in contrast to strong-rung spin ladders, this bound state is only 8 times weaker than the single magnon excitation at $q_{\parallel} = \pi$. Moreover, the two-magnon bound state seems not to be confined to a narrow q range but persists throughout about 60% of the Brillouin zone and shows itself a structured dispersion. The latter does not yet follow the expansion based on the strong-coupling approach in Ref. 36.

Being in an intermediate coupling limit with neither $x \ll 1$ nor $x \gg 1$, the observed bound state around $q_{\parallel} = \pi$ in DIMPY can hence be understood *qualitatively* either as a bound state of two dimer-triplet excitations or a bound state of two triplet and one singlet Majorana fermion excitations in the language of Ref. 41, although analytic solutions from both coupling limits cannot describe the bound-state *quantitatively* anymore.

V. CONCLUSION

In conclusion, detailed follow-up zero-field measurements on the strong-leg spin-ladder material DIMPY were performed by the neutron time-of-flight technique. The two-magnon bound state recently observed by the triple-axis scattering technique was studied in detail and shown to be persisting throughout 60% of the Brillouin zone. The structure factor of the symmetric and asymmetric excitation channel was measured and shown to be consistent with the model of two noninteracting ladder systems described by the rung vectors $\mathbf{d}_{1,2}$. It was shown how the large 4D data set collected in a time-of-flight experiment can be used in a smart way in order to sep-

arate the two channels. Moreover, the evolution of the dynamical structure factor in the strong-leg regime was studied and it was shown how both the symmetric and asymmetric channel converge towards the two-spinon continuum of a spin chain.

ACKNOWLEDGMENTS

This work is partially supported by the Swiss National Fund under division II and through Project 6 of MANEP. Research at Oak Ridge National Laboratory's Spallation Neutron Source was supported by the Scientific User Facilities Division, Office of Basic Energy Sciences, US Department of Energy. We thank Dr. Andrey Podlesnyak and the SNS sample environment team for their support during the experiment.

APPENDIX: BACKGROUND SUBTRACTION

In the following Appendix we briefly describe the background subtraction procedure. It is a standard approach and was performed in a similar way in, e.g., Refs. 3 and 42. For the present experiment, two sources of background were assumed: (1) Temperature-independent background both from the cryostat and other equipment as well as coherent and incoherent scattering from the sample²⁷ and (2) inelastic phonon scattering from the sample, proportional to the Bose factor $n(\omega) + 1$. The total signal $\mathcal{I}(\mathbf{Q}, \omega, T)$ at $T_1 = 50$ K and $T_2 = 110$ K was modeled as

$$\mathcal{I}(\mathbf{Q}, \omega, T) = \mathcal{A}(\mathbf{Q}, \omega) + \mathcal{B}(\mathbf{Q}, \omega)[n(\omega, T) + 1], \quad (\text{A1})$$

with $n(\omega) = (e^{\hbar\omega/k_B T} - 1)^{-1}$ and \mathcal{A} , \mathcal{B} describing the T -independent and T -dependent background, respectively. The background contributions can be calculated by

$$\mathcal{B}(\mathbf{Q}, \omega) = \frac{\mathcal{I}_1(\mathbf{Q}, \omega) - \mathcal{I}_2(\mathbf{Q}, \omega)}{n(\omega, T_1) - n(\omega, T_2)}, \quad (\text{A2})$$

$$\mathcal{A}(\mathbf{Q}, \omega) = \mathcal{I}_1(\mathbf{Q}, \omega) - \mathcal{B}(\mathbf{Q}, \omega)[n(\omega, T_1) + 1]. \quad (\text{A3})$$

The background subtracted signal at base temperature $T_0 = 1.5$ K is therefore

$$\mathcal{I}^{\text{sub}}(\mathbf{Q}, \omega) = \mathcal{I}_0(\mathbf{Q}, \omega) - \mathcal{A}(\mathbf{Q}, \omega) - \mathcal{B}(\mathbf{Q}, \omega)[n(\omega, T_0) + 1]. \quad (\text{A4})$$

*zhelud@ethz.ch; <http://www.neutron.ethz.ch/>

¹T. Giamarchi, *Quantum Physics in One Dimension* (Oxford University Press, Oxford, 2003).

²A. M. Tsvelik, *Quantum Field Theory in Condensed Matter Physics*, 2nd ed. (Cambridge University Press, Cambridge, 2007).

³D. C. Dender, D. Davidović, D. H. Reich, C. Broholm, K. Lefmann, and G. Aeppli, *Phys. Rev. B* **53**, 2583 (1996).

⁴M. B. Stone, D. H. Reich, C. Broholm, K. Lefmann, C. Rischel, C. P. Landee, and M. M. Turnbull, *Phys. Rev. Lett.* **91**, 037205 (2003).

⁵B. Lake, D. A. Tennant, C. D. Frost, and S. E. Nagler, *Nat. Mater.* **4**, 329 (2005).

⁶M. Klanjšek, H. Mayaffre, C. Berthier, M. Horvatić, B. Chiari, O. Piovesana, P. Bouillot, C. Kollath, E. Orignac, R. Citro, and T. Giamarchi, *Phys. Rev. Lett.* **101**, 137207 (2008).

⁷B. Thielemann, C. Rüegg, K. Kiefer, H. M. Rønnow, B. Normand, P. Bouillot, C. Kollath, E. Orignac, R. Citro, T. Giamarchi *et al.*, *Phys. Rev. B* **79**, 020408 (2009).

⁸B. Thielemann, C. Rüegg, H. M. Rønnow, A. M. Läuchli, J.-S. Caux, B. Normand, D. Biner, K. W. Krämer, H.-U. Güdel, J. Stahn *et al.*, *Phys. Rev. Lett.* **102**, 107204 (2009).

⁹V. S. Zapf, D. Zocco, B. R. Hansen, M. Jaime, N. Harrison, C. D. Batista, M. Kenzelmann, C. Niedermayer, A. Lacerda, and A. Paduan-Filho, *Phys. Rev. Lett.* **96**, 077204 (2006).

¹⁰A. Zheludev, V. O. Garlea, T. Masuda, H. Manaka, L.-P. Regnault, E. Ressouche, B. Grenier, J.-H. Chung, Y. Qiu, K. Habicht *et al.*, *Phys. Rev. B* **76**, 054450 (2007).

¹¹T. Barnes, E. Dagotto, J. Riera, and E. S. Swanson, *Phys. Rev. B* **47**, 3196 (1993).

- ¹²T. Giamarchi, C. Rüegg, and O. Tchernyshyov, *Nat. Phys.* **4**, 198 (2008).
- ¹³T. Masuda, A. Zheludev, H. Manaka, L.-P. Regnault, J.-H. Chung, and Y. Qiu, *Phys. Rev. Lett.* **96**, 047210 (2006).
- ¹⁴T. Fischer, S. Duffe, and G. S. Uhrig, *Europhys. Lett.* **96**, 47001 (2011).
- ¹⁵C. Rüegg, K. Kiefer, B. Thielemann, D. F. McMorrow, V. Zapf, B. Normand, M. B. Zvonarev, P. Bouillot, C. Kollath, T. Giamarchi *et al.*, *Phys. Rev. Lett.* **101**, 247202 (2008).
- ¹⁶P. Bouillot, C. Kollath, A. M. Läuchli, M. Zvonarev, B. Thielemann, C. Rüegg, E. Orignac, R. Citro, M. Klanjšek, C. Berthier *et al.*, *Phys. Rev. B* **83**, 054407 (2011).
- ¹⁷S. Sachdev and R. N. Bhatt, *Phys. Rev. B* **41**, 9323 (1990).
- ¹⁸S. Gopalan, T. M. Rice, and M. Sigrist, *Phys. Rev. B* **49**, 8901 (1994).
- ¹⁹F. D. M. Haldane, *Phys. Rev. Lett.* **50**, 1153 (1983).
- ²⁰E. Dagotto and T. M. Rice, *Science* **271**, 618 (1996).
- ²¹S. Notbohm, P. Ribeiro, B. Lake, D. A. Tennant, K. P. Schmidt, G. S. Uhrig, C. Hess, R. Klingeler, G. Behr, B. Büchner *et al.*, *Phys. Rev. Lett.* **98**, 027403 (2007).
- ²²A. Shapiro, C. P. Landee, M. M. Turnbull, J. Jornet, M. Deumal, J. J. Novoa, M. A. Robb, and W. Lewis, *J. Am. Chem. Soc.* **129**, 952 (2007).
- ²³J. Jornet-Somoza, M. Deumal, M. M. Turnbull, and J. J. Novoa, *Polyhedron* **28**, 1965 (2009).
- ²⁴D. Schmidiger, S. Mühlbauer, S. N. Gvasaliya, T. Yankova, and A. Zheludev, *Phys. Rev. B* **84**, 144421 (2011).
- ²⁵D. Schmidiger, P. Bouillot, S. Mühlbauer, S. Gvasaliya, C. Kollath, T. Giamarchi, and A. Zheludev, *Phys. Rev. Lett.* **108**, 167201 (2012).
- ²⁶The interladder interaction was found to be $J' \approx 6 \mu\text{eV}$, more than 2 orders of magnitude smaller than J_{leg} and J_{rung} .
- ²⁷G. L. Squires, *Introduction to the Theory of Neutron Scattering* (Cambridge University Press, Cambridge, 1978).
- ²⁸G. Ehlers, A. A. Podlesnyak, J. L. Niedziela, E. B. Iverson, and P. E. Sokol, *Rev. Sci. Instrum.* **82**, 085108 (2011).
- ²⁹T. Hong, Y. H. Kim, C. Hotta, Y. Takano, G. Tremelling, M. M. Turnbull, C. P. Landee, H.-J. Kang, N. B. Christensen, K. Lefmann *et al.*, *Phys. Rev. Lett.* **105**, 137207 (2010).
- ³⁰T. G. Perring, R. A. Ewings, and J. V. Duijn, 2009 (unpublished), <http://horace.isis.rl.ac.uk>.
- ³¹P. J. Brown, in *International Tables for Crystallography*, 3rd ed., edited by E. Prince, Vol. C (Kluwer Academic Publishers, Dordrecht, 2004), Chap. 4.4.5.
- ³²The threshold for the symmetric channel was taken to be slightly lower in order to resolve the two-magnon bound state which is much weaker than the magnon excitations.
- ³³K. Damle and S. Sachdev, *Phys. Rev. B* **57**, 8307 (1998).
- ³⁴M. Greven, R. J. Birgeneau, and U. J. Wiese, *Phys. Rev. Lett.* **77**, 1865 (1996).
- ³⁵O. P. Sushkov and V. N. Kotov, *Phys. Rev. Lett.* **81**, 1941 (1998).
- ³⁶W. Zheng, C. J. Hamer, R. R. P. Singh, S. Trebst, and H. Monien, *Phys. Rev. B* **63**, 144410 (2001).
- ³⁷M. Reigrotzki, H. Tsunetsugu, and T. M. Rice, *J. Phys.: Condens. Matter* **6**, 9235 (1994).
- ³⁸J. Oitmaa, R. R. P. Singh, and W. Zheng, *Phys. Rev. B* **54**, 1009 (1996).
- ³⁹C. Knetter, K. P. Schmidt, M. Grüninger, and G. S. Uhrig, *Phys. Rev. Lett.* **87**, 167204 (2001).
- ⁴⁰G. Müller, H. Thomas, H. Beck, and J. C. Bonner, *Phys. Rev. B* **24**, 1429 (1981).
- ⁴¹D. G. Shelton, A. A. Nersisyan, and A. M. Tsvelik, *Phys. Rev. B* **53**, 8521 (1996).
- ⁴²M. B. Stone, I. A. Zaliznyak, T. Hong, C. L. Broholm, and D. H. Reich, *Nature (London)* **440**, 187 (2006).